Martensitic Steel Microstructure Effects on Cavitation Erosion

Markku Ylönen[1,2,*], Tuomo Nyyssönen[3], Mari Honkanen[4], Pasi Peura[5]

[1]Tampere University, Mechanical Engineering and Industrial Systems, P.O. Box 589, FI-33014 Tampere University, Finland
[2]Université Grenoble Alpes, LEGI, FR-38000 Grenoble, France
[3]Outotec Research Center, P.O. Box 69, FI-28101 Pori, Finland
[4] Tampere University, Tampere Microscopy Center, P.O. Box 692, FI-33014 Tampere University, Finland
Materials Science and Environmental Engineering, P.O. Box 589, FI-33014 Tampere University, Finland
[*]Corresponding author: markku.ylonen@tuni.fi

Abstract

Cavitation and cavitation erosion are sometimes unavoidable phenomena in hydro machine operation. For example, operating hydro turbines as regulating power leads to situations where the risk of cavitation is accepted to some extent. Cavitation resistant materials are therefore required to reduce machine damage and maintenance. This study characterizes the microstructure of two martensitic stainless steels from Francis turbines. They were already studied for cavitation erosion resistance in a previous study, and this study reveals the reasons behind the other steel having a significantly better resistance, while they had similar chemical compositions. The electron backscatter diffraction (EBSD) method is effective in defining the martensitic microstructure, specifically the block, packet and prior austenite grain level. In addition, the retained austenite is effectively detected with the method. A fine prior austenite grain size and small packet and block sizes were found to be among the defining factors in cavitation erosion resistance of these steels. In addition, the transformation of retained austenite to martensite was detected in the edge region where cavitation had taken place. This transformation further increases cavitation erosion resistance. The better resistance of Steel 1 against cavitation was attributed to these microstructural differences. According to these findings, the microstructure in Steel 1 would be highly beneficial in building cavitation erosion resistant hydro machines, and would be of interest to manufacturers of martensitic stainless steel components.

Keywords: Cavitation erosion resistance, martensitic steel microstructure, electron backscatter diffraction

Nomenclature

EBSD = Electron Backscatter Diffraction

IPF = Inverse Pole Figure

PAG = Prior Austenite Grain

SEM = Scanning Electron Microscope

1. Introduction

Cavitation is a phenomenon where vapor bubbles form in a static or moving liquid due to a local drop in pressure. When these microscopic vapor bubbles collapse near a material surface, they cause local damage. Successive impacts lead to cavitation erosion, which is a major wear mechanism of many

hydro machines. As the hydro machines are sought to operate at high performance, cavitation may not always be avoided by flow channel design and operational limits. Therefore, material choices may play an important role in machine life cycle. Our earlier study[1]already included SEM and optical microscopy, to study material composition and to characterize the erosion process. However, the reason behind the erosion rate differences was not conclusively identified.

Martensitic stainless steels exhibit high strength and relatively good corrosion resistance, providing an attractive combination of properties for offshore marine applications that require high structural performance in a saline water environment. The martensitic microstructure is composed of nanoscale-sized laths formed during cooling in a high-temperature parent austenite phase by a shear transformation. The resulting microstructure has been considerably refined compared to the parent austenite microstructure, resulting in improved mechanical properties.

Every martensitic lath has a strictly determined crystallographic orientation relationship with their parent austenite grain, sharing certain near-parallel planes and orientations[2]. The laths are typically organized into blocks, which in turn are organized into packets. The blocks are composed of lath pairs with a low disorientation angle. The microstructure of martensite therefore may not be easily quantified simply in terms of grain size. However, correlations between block and packet size and various mechanical properties have been observed in numerous studies[3–5]. The difficulty usually lies in determining the boundaries of blocks and packets, which is often difficult with traditional methods such as optical metallography. Electron backscatter diffraction (hereafter referred to as EBSD), a method for determining orientation maps for crystalline sample surfaces, has emerged as a powerful method for quantifying and examining the martensitic microstructure (as well as crystallography) at a block, packet and prior austenite grain level[6, 7].

This advances further in the analysis than the previous study[1], where two different stainless steels used in Francis turbine runner blades were subjected to cavitation erosion. Steel 1, which was from a turbine commissioned in the 1970s, had a significantly higher cavitation erosion resistance compared to Steel 2, which was taken from a turbine commissioned in the 2010s. The microstructures of both steels were martensitic. The result of the cavitation experiments was a surprise, as a modern material performed worse. Additional studies were therefore needed to highlight the reasons behind the observed resistance of Steel 1 to cavitation damage. The present studies concentrated on the EBSD method. It is an additional characterization technique employed with a scanning electron microscope (SEM) giving a crystallographic information from a sample surface. It can be utilized to study e.g. individual grain orientations, local texture, and phase identification and distribution mainly in polycrystalline materials[8].

2. Experiments

2.1 EXPERIMENTAL PROGRAM

The cavitation tunnel used in this study was a water loop that generates an axisymmetric cavitation erosion pattern on a cylindrical sample. The other circular face of the 100 mm diameter and 20 mm thick cylindrical sample experienced cavitation erosion. The main features of the tunnel are: 1) the test section that is a nozzle directed on a sample, with flow stagnation on the sample surface and then a radially diverging channel, 2) a downstream tank for overall control of tunnel pressure, and 3) a frequency regulator controlled pump to adjust upstream pressure. Cavitation inception occurs at the nozzle exit, as the cross section area drops when shifting to the radial section. Cavitation closure occurs about 20 mm further downstream, in the radially diverging section, as the static pressure

recovers. The tunnel operation is explained in more detail in the previous works by Ylönen et al. and by Chahine, Franc and Karimi and Franc[1, 9, 10].

The erosion properties of the materials were already presented in the previous study[1]. As this study focuses on the reasons behind the varying cavitation erosion resistances, the in-depth erosion rate analysis and the cavitation testing scheme are excluded. The erosion rates were expressed as volume loss rates, and they were calculated as an average from the surface profiles of all the eight different specimen azimuthal angles that were measured, using a contact profilometer. The erosion rates were:

- 1.79 mm^3/h for Steel 1

- 2.72 mm^3/h for Steel 2

According to the averaged volume loss rates, Steel 2 eroded about 50 % faster than steel 1. Both of them were eroded for 65 hours, and the erosion rates were defined in the steady state erosion regime. This study focuses on the material microstructures behind this difference. The approach in this study was to utilize SEM (ULTRAplus, Zeiss) equipped with an EBSD system (Symmetry EBSD detector based on CMOS technology with AZtecHKL software, Oxford Instruments).

2.2 MATERIAL COMPOSITIONS

The material chemical compositions, measured using an optical spectrometer (ARL 4460 Optical Emission Spectrometer), are listed in Table 1. The chemical compositions of the steels are very similar, the biggest differences being the addition of approximately 0.1 wt-% tungsten in Steel 1, a higher carbon content and lower molybdenum content.

Table 1. Material chemical compositions as a percentage.

Material	Fe	C	Cr	Si	Mn	P	S	Ni	Mo	W
Steel 1	80.1	0.04	12.8	0.3	0.7	0.03	0.02	5.4	0.3	0.1
Steel 2	81.1	0.02	12.8	0.4	0.6	0.03	0.004	4.2	0.5	0.002

Initially, the microstructure was studied using optical microscopy of polished and etched specimens[1]. The etchant was Vilella's Reagent. It was observed that the microstructure of the steels consists of lath martensite, with a small amount of intercritical ferrite and various smaller carbides and other particles. The etching procedure resolved the prior austenite grain boundaries for Steel 1, whose prior austenite grain size was determined by the lineal intercept method as determined by ASTM E112-13, *Standard Test Methods for Determining Average Grain Size*[11]. The measured grain size was 37 μm with a standard deviation of 10 μm. Steel 2, however, did not reveal its primary austenite grain boundaries by this method. Based on lath and packet morphology resolved through optical microscopy, the grain size was estimated to be much larger, possibly by an order of magnitude.

2.3 EBSD DATA HANDLING

The EBSD orientation maps were collected in order to obtain block, packet and prior austenite grain boundaries as well as determine the possible presence of retained austenite in the microstructure of the steels. The analyzed specimens were sectioned from the cavitation samples, ground and polished with 0.1μm colloidal silica used in the final polishing step. Three EBSD orientation maps were acquired (acceleration voltage 20 kV) for each specimen: one map from the bulk microstructure of the specimen and two maps from the cavitated edge regions. For both steels, three maps of dimensions 226.4x169.8 μm were taken at a step size of 0.4 μm. An additional map at a resolution of 0.2 μm was taken for both steels to ensure that no details were lost due to the relatively large step size. The indexed phases

were ferritic (bcc) and austenitic (fcc) iron. In all cases, the indexing hit rate was in excess of 85 %, with non-indexed regions situated at grain or lath boundaries. The data was cleaned by removing single-pixel orientation measurements (no neighboring orientation pixels with a larger disorientation angle than 3 degrees). A grain map was reconstructed from the data using an angular threshold of 3 degrees.

The martensitic lath boundaries were resolved from the acquired maps by using the iterative orientation relationship determination algorithm described in the works by Stormvinter et al. and Nyyssönen et al.[7, 12]. After determining the best representative orientation relationship between austenite and martensite for the entire dataset, each misorientation between the average orientations of all grain pairs was indexed according to the notation used by Morito et al.[2]. Following this notation, the first six misorientations correspond to the misorientations between variants in the same packet. In essence, the block, packet and prior austenite grain boundaries were resolved from each orientation map. The algorithm was implemented as Matlab® scripts using the MTEX crystallography analysis toolbox[13].

3. Results

3.1 BULK MICROSTRUCTURE

Fig. 1 shows representative images of the band contrast maps (representing the quality of the Kikuchi diffraction pattern for each measurement pixel) for both specimens, overlaid with retained austenite grains (inverse pole figure (IPF) Z direction coloring, colors correspond to the crystallographic plane of austenite parallel to the observed plane). Surprisingly, a high amount of retained austenite was present in the microstructure of Steel 1. In the image (Fig. 1a), the reconstructed austenite grains are clearly organized into clusters by IPF coloring. The shared color indicates a similar crystallographic orientation for these grains and shows that they have shared the same prior austenite grain. The boundaries highlighted in black indicate the boundaries of these original prior austenite grains and the red boundaries the packet boundaries. The retained austenite can be found uniformly within packets at block boundaries, at packet boundaries and prior austenite grain (PAG) boundaries. Conversely, Steel 2 (Fig. 1b) did not have any retained austenite and additionally has a much larger prior austenite grain size as indicated by the black boundaries. Finally, a ferrite (α) grain is visible in the upper portion of the band contrast image.

The average prior austenite grain size was 37 ± 10 µm for Steel 1 and 72 ± 20 µm for Steel 2, measured from the processed orientation maps with the lineal intercept method determined by ASTM E112[11]. The lineal intercept method is most suited for the characterization of reasonably equiaxed and uniformly sized ferritic or austenitic grain structures. As discussed by Lehto et al.[14], its use is problematic when the grain structure has a broad size distribution or a non-equiaxed morphology. The characterization of the block and packet morphology was instead done using the point intercept method, demonstrated by Lehto et al.[14]. Table 2 shows the measured block and packet sizes, as well as the austenite grain size. It should be noted that the retained austenite grain boundaries were not omitted from either the block or the packet size determination for Steel 1. In addition, Table 2 shows the retained austenite fraction measured directly from the orientation map measured for Steel 1 at a step size of 0.2 µm.

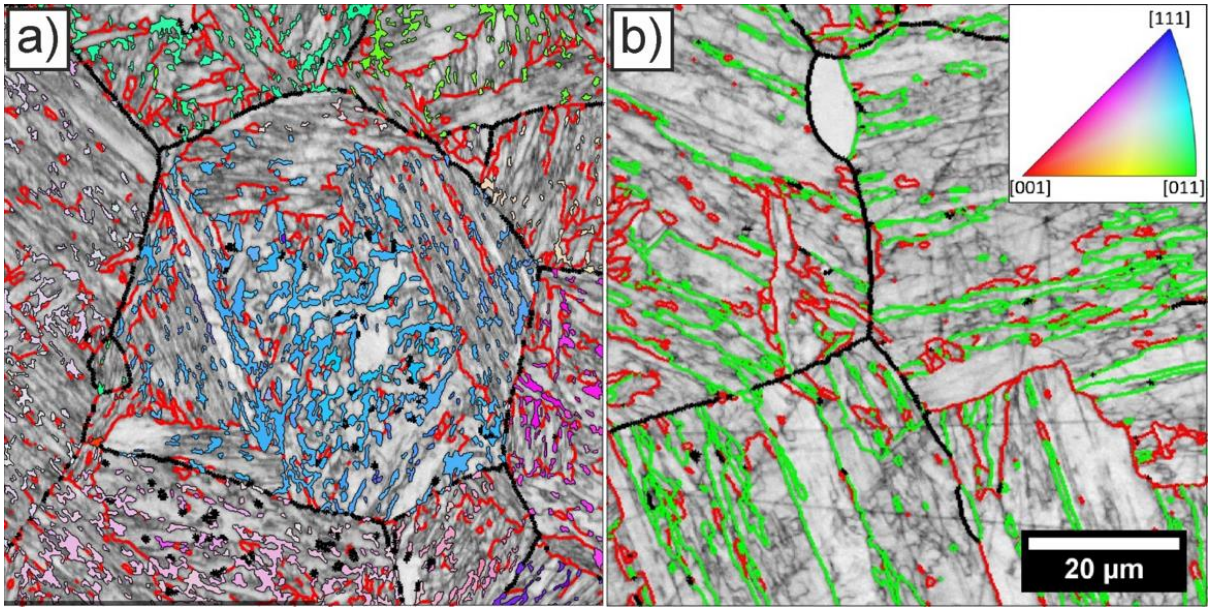

Figure 1. Representative band contrast maps overlaid with IPF Z colored reconstructed austenite grains, as well as block (green), packet (red) and prior austenite (black) boundaries for (a) Steel 1 and (b) Steel 2. The block boundaries have been omitted for Steel 1 for clarity. The IPF Z color key and the scale bar for both images are shown in Fig. 1b.

Table 2. The measured austenite fraction for Steel 1, the prior austenite grain size measured with the lineal intercept method[11] and the prior austenite, packet and block sizes measured with the point intercept method[14]. For the lineal intercept PAG size, the reported error is the standard deviation of the measured values. For the point intercept values, the reported values are the mean and the 5 % and 95 % quantiles of the measured values.

EBSD indexation	**Steel 1**			**Steel 2**		
γ fraction [vol-%]	9			-		
Prior γ grains analyzed following boundary indexation	124			11		
ASTM E112 lineal intercept[11]	**Steel 1**			**Steel 2**		
PAG size [µm]	37 ± 10			72 ± 20		
Point intercept[14]	**Steel 1**			**Steel 2**		
	5 %	**mean**	95 %	5 %	**mean**	95 %
PAG size [µm]	9.1	**40.2**	71.2	27.0	**108.6**	214.7
Packet size [µm]	0.6	**4.1**	10.8	2.1	**19.8**	51.6
Block size [µm]	0.4	**2.8**	7.4	1.1	**11.2**	32.2

In Steel 2, the martensite is fairly typical lath martensite with a large amount of V1-V2 type high-angle 60 ° twin boundaries and V1-V4 type low-angle boundaries[2]. The fraction of V1-V4 type boundaries may be underestimated based on the dark lines in the band contrast image in Fig. 1b where no lath boundary has been found. In these cases, the local boundary between two laths has such a low disorientation angle (typical to V1-V4) that the laths cannot be distinguished from each other based on crystallographic analysis. Dislocations can be transmitted across these types of boundaries more easily and they do not contribute to the strength of the material in a similar manner as high-angle grain boundaries[15]. Conversely, the interphase boundaries between martensite and austenite in Steel 1 offer a significant obstacle to dislocation movement, thus strengthening the microstructure.

3.2 EDGE REGIONS

Besides effective grain refinement, another important aspect contributing to the better performance of Steel 1 could be the strain-induced transformation of retained austenite to martensite during the plastic deformation caused by cavitation. For low-alloy and stainless steels, this phenomenon combined with this type of microstructure has been demonstrated to lead to very favourable strength-ductility combinations[16, 17].

Fig. 2 shows the eroded edge regions of the specimens. For both steels, the amount of prior austenite grain boundaries (shown in black) and packet boundaries (red) appears to increase when approaching the edge. This is in fact a sign that the prior austenite grain boundary indexing has failed due to the additional intragrain rotations caused by plastic deformation that has taken place in the edge regions as the result of cavitation. The black and red boundaries in the region within 30 μm cannot therefore be considered realistic packet and PAG boundaries. The cavitation erosion process is assumed to be low-cycle fatigue locally exceeding the yield point of the steel, so the observed deformation is as expected[1].

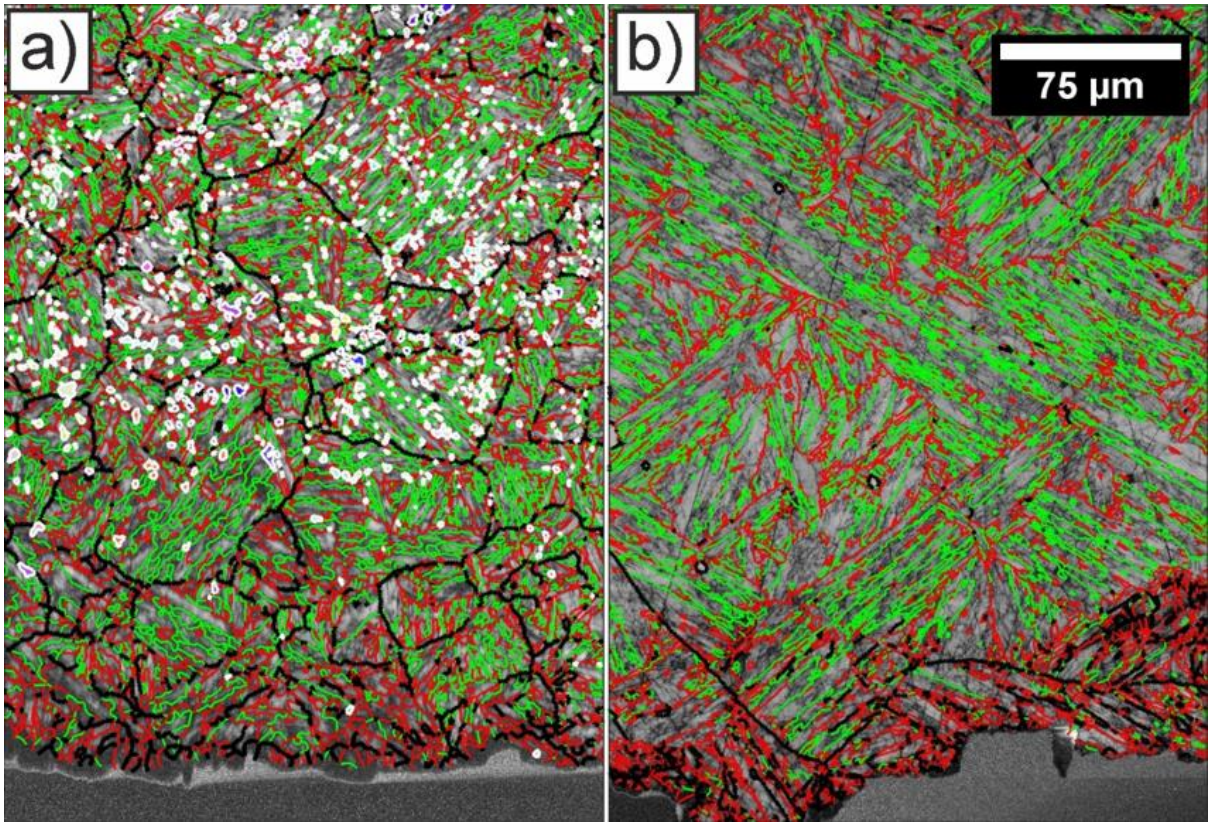

Figure 2. EBSD band contrast images with superimposed boundaries for prior austenite (black), packets (red) and blocks (green), as well as IPF Z orientation colored retained austenite grains highlighted with white boundaries for (a) Steel 1 and (b) Steel 2. For orientation coloring, refer to the color key in Fig. 1b. The scale bar for both images is in Fig. 2b.

Fig. 2a shows retained austenite grains highlighted with white boundaries. The retained austenite is not present in the edge regions, indicating the possibility that strain-induced transformation of austenite to martensite has taken place. This type of transformation would contribute significantly to strain hardening, improving the resistance of the material towards cavitation. Fig. 3 shows the evolution in the fraction of retained austenite quantitatively when approaching the eroded edge (taken as an average fraction over the horizontal direction in steps of 4 μm). The amount of retained

austenite evens out at a value of 2 vol-% at approximately 200 µm from the eroded edge in Fig. 3. The low evened-out austenite fraction compared to the bulk measurement (9 vol-%) is explained by the step size of 0.4 µm in the orientation maps of Fig. 2 and Fig. 3 compared to the 0.2 µm in the orientation map of Fig. 1 showing the bulk material. For comparison, retained austenite could not be detected in the bulk at all in Steel 2 at a step size of 0.4 µm.

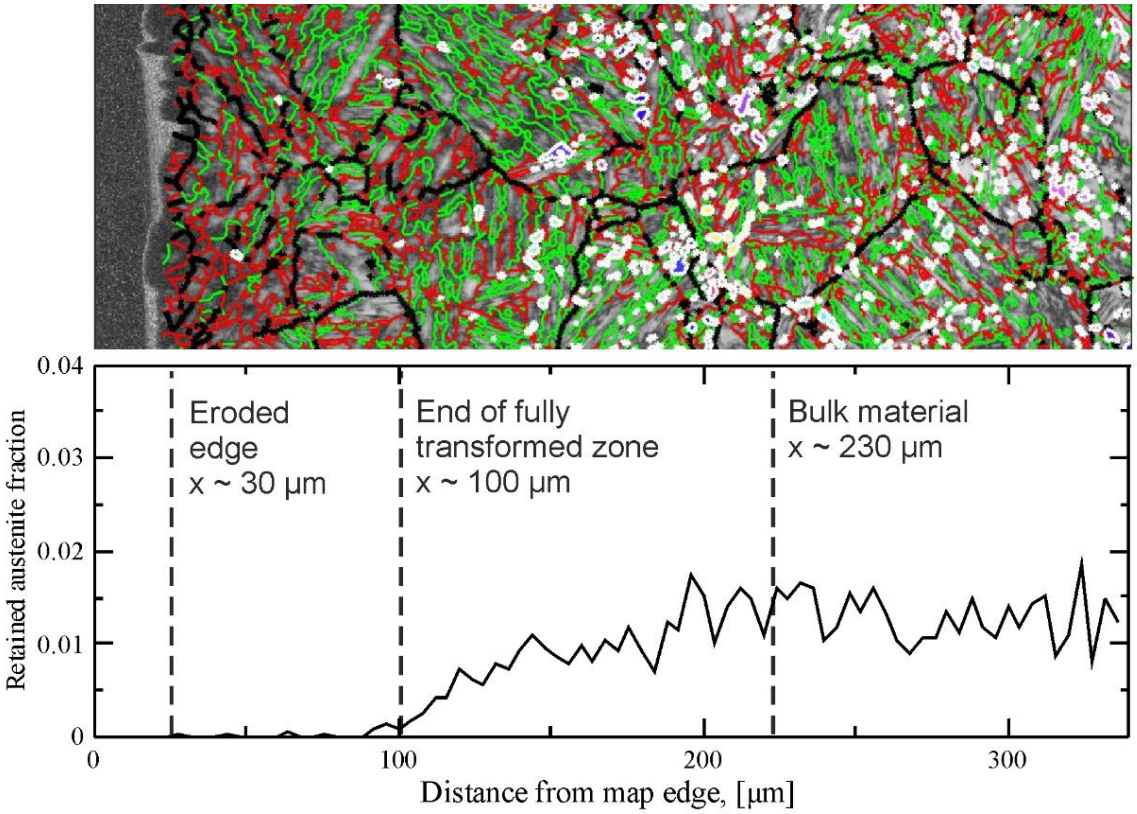

Figure 3. Retained austenite fraction shown with respect to the distance from the map edge. A cropped and rotated section of the orientation map used for the measurement (the map from Fig. 2a) is shown above for visualization purposes, scaled to match the coordinates of the graph.

Berchiche, Franc and Michel[18] reported a 200-µm depth for a completely strain-hardened layer for stainless steel 316L that had experienced cavitation erosion. They measured it through micro-hardness of a cut sample. The strain hardening depth was measured for an eroded sample that had already experienced material loss. The material was not exactly the same as in this study, but it is similar enough to deduce with high certainty that the retained austenite profile in the eroded area in Fig. 3 corresponds to the strain-hardened area.

4. Conclusions

The microstructure of the steels was confirmed to consist of lath martensite, with a significant amount of retained austenite in Steel 1. The prior austenite grain size for Steel 2 is very large, as expected based on the previous study. The large grain size and the correspondingly low amount of grains analysed in the collected EBSD maps is reflected in the high quantified uncertainties reported in Table 2. However, it could be confirmed that the prior austenite grain size of Steel 1 is considerably finer than that of Steel 2. Correspondingly, the block and packet sizes are significantly finer as well. The retained austenite in Steel 1 resides as fine particles within the block structure, providing a further refining element. The fraction of retained austenite was found to gradually diminish at the edge regions. This is likely an indication of a strain-induced martensitic transformation, which would

contribute to strain hardening of the material during cavitation erosion. The strain-hardened layer thickness corresponds to that of Berchiche, Franc and Michel[18], thus indicating that the retained austenite profile also reveals the strain hardening. Based on the studies here, it is concluded that the better performance of Steel 1 in the cavitation tests is due to a combination of a more refined microstructure compared to Steel 1 and the transformation-aided strain hardening during cavitation.

The presence of retained austenite in the microstructure of Steel 1 is intriguing. Based on the alloying content, both steels should have an M_s of approximately 350 °C[19], in which case they should become completely martensitic when quenched to room temperature. A more accurate analysis of the alloying content (with an emphasis on measuring the carbon content) could provide more insight into the fabrication process of Steel 1 and possibly open new avenues for the production of cavitation-resistant stainless steel microstructures. One possibility is that the alloy has been intercritically annealed following quenching, which in a previous study by Song et al.[20] has been shown to result in similar microstructure as observed here.

Acknowledgements

This work made use of Tampere Microscopy Center facilities at Tampere University. The authors would like to thank Business Finland, Fortum Power and Heat Oy, Sandvik Mining and Construction Oy, Valtra Oy, and Teollisuuden Voima Oyj and Fortum Foundation for funding the research and for providing technical support.

References

1. M. Ylönen, P. Saarenrinne, J. Miettinen, J-P. Franc, M. Fivel, T. Nyyssönen, "Cavitation Erosion Resistance Assessment and Comparison of Three Francis Turbine Runner Materials," *Materials Performance and Characterization 7*, no. 5, (November 2018): 1107-1126, https://doi.org/10.1520/MPC20180015

2. S. Morito, H. Tanaka, R. Konishi, T. Furuhara, T. Maki, "The morphology and crystallography of lath martensite in Fe-C alloys," *Acta Materialia 51*, no. 6, (April 2003): 1789-1799, https://doi.org/10.1016/S1359-6454(02)00577-3

3. T. Hanamura, T. Yin, K. Nagai, "Ductile-Brittle Transition Temperature of Ultrafine Ferrite/Cementite Microstructure in a Low Carbon Steel Controlled by Effective Grain Size," *ISIJ Int 44*, no. 3, (March 2004): 610–617, https://doi.org/10.2355/isijinternational.44.610

4. C. Wang, M. Wang, J. Shi, W. Hui, H. Dong, "Effect of microstructural refinement on the toughness of low carbon martensitic steel," *Scr Mater 58*, no. 6, (March 2008): 492–495, https://doi.org/10.1016/j.scriptamat.2007.10.053

5. Jr. J.W. Morris, "On the Ductile-Brittle Transition in Lath Martensitic Steel," *ISIJ Int 51*, no. 10, (October 2011): 1569–1575, https://doi.org/10.2355/isijinternational.51.1569

6. T. Nyyssönen, P. Peura, V-T. Kuokkala, "Crystallography, Morphology, and Martensite Transformation of Prior Austenite in Intercritically Annealed High-Aluminum Steel," *Metallurgical and Materials Transactions A 49*, no. 12, (December 2018): 6426-6441, https://doi.org/10.1007/s11661-018-4904-9

7. A. Stormvinter, G. Miyamoto, T. Furuhara, P. Hedström, A. Borgenstam, "Effect of carbon content on variant pairing of martensite in Fe–C alloys," *Acta Materialia 60*, no. 20, (December 2012): 7265-7274, https://doi.org/10.1016/j.actamat.2012.09.046

8. R. Schwarzer, D. Field, B. Adams, M. Kumar, A. Schwartz, “Present State of Electron Backscatter Diffraction and Prospective Developments,” in *Electron Backscatter Diffraction in Materials Science*, ed. A. Schwartz, M. Kumar, B. Adams, D. Field (Boston, MA: Springer 2009), 1-20. https://doi.org/10.1007/978-0-387-88136-2_1

9. G. Chahine, J-P. Franc, A. Karimi, “Laboratory Testing Methods of Cavitation Erosion,” in *Advanced Experimental and Numerical Techniques for Cavitation Erosion Prediction*, ed. K-H. Kim, G. Chahine, J-P. Franc, A. Karimi (Heidelberg, Germany: Springer Dordrecht Heidelberg 2014), 21-35. https://doi.org/10.1007/978-94-017-8539-6

10. J-P. Franc, “Incubation Time and Cavitation Erosion Rate of Work-Hardening Materials,” *Journal of Fluids Engineering 131*, no. 2, (February 2009): 021303, https://doi.org/10.1115/1.3063646

11. *Standard Test Methods for Determining Average Grain Size,* ASTM E112-13, (West Conshohocken, PA: ASTM International, 2013), https://doi.org/10.1520/E0112-13

12. T. Nyyssönen, M. Isakov, P. Peura, V-T. Kuokkala, “Iterative Determination of the Orientation Relationship Between Austenite and Martensite from a Large Amount of Grain Pair Misorientations,” *Metallurgical and Materials Transactions A 47*, no. 6, (June 2016): 2587-2590, https://doi.org/10.1007/s11661-016-3462-2

13. F. Bachmann, R. Hielscher, H. Schaeben, “Texture Analysis with MTEX - Free and Open Source Software Toolbox,” *Solid State Phenomena 160*, (February 2010): 63-68, https://doi.org/10.4028/www.scientific.net/SSP.160.63

14. P. Lehto, J. Romanoff, H. Remes, T. Sarikka, “Characterisation of local grain size variation of welded structural steel,” *Weld World 60*, no. 4, (July 2016): 673-688, https://doi.org/10.1007/s40194-016-0318-8

15. B. Liu, P. Eisenlohr, F. Roters, D. Raabe, “Simulation of dislocation penetration through a general low-angle grain boundary,” *Acta Materialia 60*, no. 13–14, (August 2012): 5380–5390, https://doi.org/10.1016/j.actamat.2012.05.002

16. Q. Huang, C. Schröder, H. Biermann, O. Volkova, J. Mola, “Influence of Martensite Fraction on Tensile Properties of Quenched and Partitioned (Q&P) Martensitic Stainless Steels,” *steel research international 87*, no. 8, (August 2016): 1082-1094, https://doi.org/10.1002/srin.201500472

17. J. Speer, A. Streicher, D. Matlock, F. Rizzo, G. Krauss, “Quenching and partitioning: A fundamentally new process to create high strength trip sheet microstructures,” (paper presentation, *Materials Science and Technology 2003 Meeting*, Chicago, IL, November 9-12, 2003): 505-522

18. N. Berchiche, J-P. Franc, J. Michel, “A Cavitation Erosion Model for Ductile Materials,” *Journal of Fluids Engineering 124*, no. 3, (September 2002): 601-606, https://doi.org/10.1115/1.1486474

19. K. Andrews, “Empirical Formulae for the Calculation of Some Transformation Temperatures,” *The Journal of the Iron and Steel Institute 203*, (1965): 721-727

20. P. Song, W. Liu, C. Zhang, L. Liu, Z. Yang, “Reversed Austenite Growth Behavior of a 13%Cr-5%Ni Stainless Steel during Intercritical Annealing”, *ISIJ International 56*, no. 1, (January 2016): 148-153, https://doi.org/10.2355/isijinternational.ISIJINT-2015-280

List of Figures

Figure 1. Representative band contrast maps overlaid with IPF Z colored reconstructed austenite grains, as well as block (green), packet (red) and prior austenite (black) boundaries for (a) Steel 1 and (b) Steel 2. The block boundaries have been omitted for Steel 1 for clarity. The IPF Z color key and the scale bar for both images are shown in Fig. 1b.

Figure 2. EBSD band contrast images with superimposed boundaries for prior austenite (black), packets (red) and blocks (green), as well as IPF Z orientation colored retained austenite grains highlighted with white boundaries for (a) Steel 1 and (b) Steel 2. For orientation coloring, refer to the color key in Fig. 1b. The scale bar for both images is in Fig. 2b.

Figure 3. Retained austenite fraction shown with respect to the distance from the map edge. A cropped and rotated section of the orientation map used for the measurement (the map from Fig. 2a) is shown above for visualization purposes, scaled to match the coordinates of the graph.